



Scaling of Flows Over Realistic Urban Geometries: A Large-Eddy Simulation Study

Wai-Chi Cheng^{1,2} · Ying Yang¹

Received: 24 April 2022 / Accepted: 8 September 2022 / Published online: 24 September 2022
© The Author(s), under exclusive licence to Springer Nature B.V. 2022

Abstract

A large-eddy simulation (LES) method is used to investigate the characteristics and scaling of flows over realistic urban geometries. The LES method is first validated with wind-tunnel measurements for the flow over a staggered array of cubes and the grid dependence behaviour of the LES is tested. It is then applied to simulate the flows over four different realistic urban surfaces with sizes of about 1000 m × 500 m. After examining the overall flow patterns and turbulence characteristics, the time- and horizontally space-averaged profiles for the four cases are investigated. It is found that, in all cases, the vertical profiles of the mean streamwise velocity component can be characterized by an inflection point which can be identified as the height of the urban canopies. A new simple method is then proposed to predict this height for the realistic urban canopies based on the plan area fraction of the surfaces. By using this urban canopy height as the normalization length scale for the flows over realistic urban geometries, it is found that the vertical profiles of the dispersive stress, effective mixing length, and sectional drag coefficient show similar patterns as those of uniform height idealized urban canopies. This result would be useful for the development of urban flow parametrizations.

Keywords Large-eddy simulation · Mean vertical profiles · Realistic urban geometries · Urban canopy height · Urban flow parametrizations

1 Introduction

The study of urban flows is important for predicting the urban wind environment and to develop urban surface parametrizations for meso-scale weather forecasting and air quality models. Among different factors, building morphology plays an important role in the urban

✉ Wai-Chi Cheng
zhengwzh7@sysu.edu.cn

Ying Yang
yangy387@mail2.sysu.edu.cn

¹ School of Atmospheric Sciences, and Guangdong Province Key Laboratory for Climate Change and Natural Disaster Studies, Sun Yat-sen University, Zhuhai, China

² Key Laboratory of Tropical Atmosphere-Ocean System (Sun Yat-sen University), Ministry of Education, Zhuhai, China

flow characteristics. Over the years, many efforts have been put to investigating the quantitative relationship between urban flow statistics and urban morphological parameters.

In the literature, there are a large number of studies which considered idealized urban-like surfaces represented by two-dimensional street canyons or three-dimensional arrays of building blocks (Li et al. 2006; Barlow and Coceal 2009; Castro 2017). The advantage of considering idealized building configurations is that it allows for the systematic control of the morphological parameters. In the past decades, various parametrizations of urban flows have been proposed. These include the parametrizations of aerodynamic roughness length (z_0) and displacement height (d) that are based on the plan area density (λ_p) and the frontal area density (λ_f) (Macdonald et al. 1998; Grimmond and Oke 1999). In addition to the parametrizations of aerodynamic parameters, results from idealized urban geometries have been also used to develop simplified urban canopy models (UCMs) to predict the time- and horizontally space-averaged wind profiles (Macdonald 2000; Coceal and Belcher 2004; Santiago and Martilli 2010; Di Sabatino et al. 2008; Nazarian et al. 2020; Cheng and Porté-Agel 2021) by parametrizing the turbulent momentum flux and the sectional drag coefficient (C_d) within urban canopies. However, despite these models being able to reasonably parametrize the aerodynamic parameters and the flows within idealized urban canopies, how to extend these models to the complex realistic urban morphologies is still not well understood.

The height of urban canopies is an important parameter for urban flow parametrizations, which is needed to normalize the vertical coordinate. However, the definition of this height for urban canopies with non-uniform building height is not straightforward. A reasonable suggestion to identify urban canopy height is based on the location of the inflection position in the mean wind profile (Oke et al. 2017), which can be interpreted as the location of dynamical instability for plane mixing layers (Raupach et al. 1996). Xie et al. (2008) used a large-eddy simulation (LES) method to consider the flow over a staggered array of random height building blocks. They found that the inflection point in the mean wind profile is located at a height greater than the mean building height (H_{aver}) while turbulent shear stress peaks at the height of the tallest building (H_{max}). Later, using the building map data of Tokyo and Nagoya in Japan, Kanda et al. (2013) performed 100 sets of building-resolved LESs to consider the parametrizations of z_0 and d for realistic urban surfaces. Different from Xie et al. (2008), the turbulent shear stress is found to peak at somewhere between H_{aver} and H_{max} in their LES results. Besides, they found that simply extending the z_0 and d models of Macdonald et al. (1998) using H_{max} or H_{aver} as the normalizing length scale does not give satisfactory results. Instead, they proposed new models for z_0 and d , which also considered the building height standard deviation (σ_H). Based on the LES results of flow over a suite of 56 synthetic urban-like topographies, Zhu et al. (2017) further found that z_0 has a non-negligible dependence on the skewness of the urban surface topography. This is consistent with Sützl et al. (2021) who claimed that only considering σ_H and H_{max} may not be sufficient to predict z_0 and d accurately for different building configurations. Giometto et al. (2016) performed building-resolved LESs of flow over a realistic urban geometry in the city of Basel, Switzerland. They found that the height of the inflection point and maximum turbulent shear production are located at a height above H_{aver} while the dispersive stress is peaked at H_{aver} .

In addition to identifying the height of urban canopies, the impacts of urban morphology heterogeneity on the effective mixing length (l_m) and C_d within urban canopies have also drawn more attention recently. The earlier UCMs proposed by Macdonald (2000), Coceal and Belcher (2004) assumed that l_m is nearly uniform within dense urban canopies, which has recently been shown to be different from those calculated from direct numerical simulation (DNS) and LES results (Kono et al. 2010; Cheng and Porté-Agel 2015; Castro 2017). For uniform height urban canopies, a local minimum of the l_m vertical profiles is found at the urban

canyon roof level while a maximum is found at about the middle height of the urban canopies. Recently, a new UCM is proposed for uniform height urban canopies, which assumes that l_m increases linearly with the distance from the canopy roof level with a proportionality constant of about 0.8 (Cheng and Porté-Agel 2021). However, further development of the UCM is still needed to predict the flows over realistic urban geometries.

Concerning urban canopies with non-uniform building height, Yoshida and Takemi (2018) found that more than one local minimum of l_m can exist for building block arrays with variable heights. This agrees with the recent study by Blunn et al. (2022) who investigated the LES datasets of idealized urban canopy flows with variable building heights. They identified that l_m can have multiple local minimums at positions corresponding to the roof-level of buildings of different heights. However, they found that the flows in the lower region of the urban canopies could be sheltered from the shear layer formed at the roof level of the taller buildings. Currently, there are only very limited results on the l_m profile within realistic urban canopies. Based on the Reynolds-averaged Navier–Stokes (RANS) simulation results of the flow over a realistic urban geometry in Hong Kong, Cheng et al. (2021) found that l_m within the canopy shows similar general patterns as those found in idealized urban canopies with a local minimum found at the roof level of the highest building.

There are currently only very limited results on C_d in urban canopies with non-uniform heights. Based on the LES results of flows over idealized heterogeneous urban morphologies, Sützl et al. (2021) proposed a parametrization of the drag distribution by defining a generalized frontal area index. Besides, Cheng et al. (2021) found that, for the realistic urban geometries, the drag is mostly exerted in the lower urban roughness sublayer (RSL) by the dense shorter buildings instead of the particularly tall buildings.

In order to overcome the above-mentioned research challenges on the parametrization of urban flows, this study is conducted to investigate the flow characteristics over different realistic urban geometries using a building-resolved LES method. The objectives are to understand the impacts of urban geometry heterogeneity on urban flows and to provide useful information for urban flow parametrizations. In Sect. 2, the LES method is introduced and its results are validated with the wind-tunnel measurements of Cheng and Castro (2002) for the flow over a uniform staggered array of cubes. In Sect. 3, the LES results of flows over four realistic urban morphology models are discussed. In Sect. 4, the results are summarized and conclusions are drawn.

2 Large-Eddy Simulation Method and Validation

The open-source computational fluid dynamics (CFD) code OpenFOAM v1806 (OpenFOAM 2018), developed based on the finite volume method, is used in this study to perform the LESs. Similar methods have been used and validated in our previous studies for flows over two-dimensional street canyons (Cheng and Liu 2011) and over a realistic urban geometry in Hong Kong (Yao et al. 2022). Detailed descriptions of the LES method can be found in the references. In this section, the performance and grid sensitivity of the LES method are further tested against the wind tunnel measurements of Cheng and Castro (2002) for the flow over a uniform staggered array of cubes.

Figure 1 shows the computational domain for the LES validation case. In order to compare with the wind-tunnel measurements of Cheng and Castro (2002), the flow over a staggered array of cubes with λ_p equal to 0.25, similar with the experiment, is considered. Incompressible flows and isothermal conditions are considered. The size of the domain is

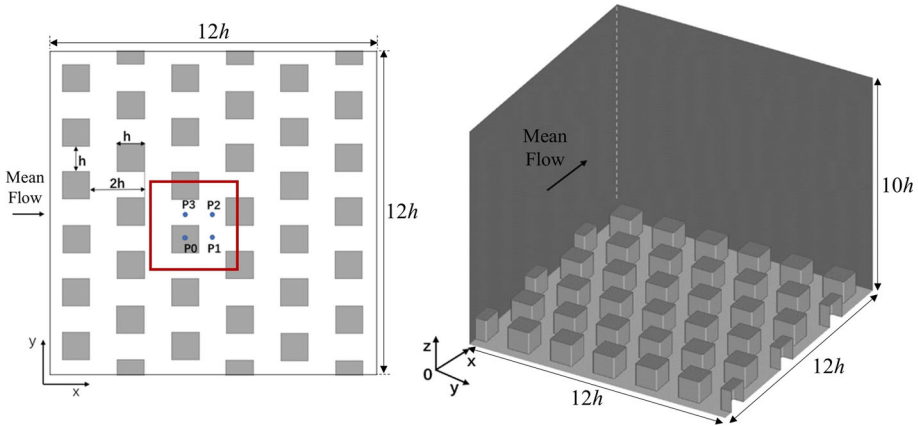


Fig. 1 Computational domain for the LES validation case

$L_x \times L_y \times L_z = 12h \times 12h \times 10h$ where $h = 20$ mm is the height of the cubes. Structured mesh composed of hexahedral volume elements with uniform resolutions in the streamwise (x), spanwise (y), and vertical (z) directions are used throughout the computational domain. The top boundary is considered as a stress-free wall. Periodic boundary conditions are used in the horizontal directions with a uniform force F_x prescribed in the x direction throughout the fluid to drive the flow. The ground and building surfaces are no-slip walls. A wall function with $z_0 = 0.002h$ is used to parametrize the wall shear stress (Spalding 1962). The subgrid-scale (SGS) stresses are parametrized using the one-equation SGS model (Schumann 1975). To test the grid sensitivity of the LES results, three different grid resolutions are considered with the number of grid points per building edge (with length h) equal to 12 (coarse), 16 (medium), and 20 (fine). Flow statistics are collected after the LESs attain the quasi-steady state. In the following results, the subgrid-scale contributions are not included and notations for filtered variables of the LESs are skipped for simple presentations.

About the numerical methods, the second-order backward scheme is used in the time integration. The least-squares gradient scheme and the linear-upwind stabilized transport divergence scheme is used to calculate the gradient and the divergence terms, respectively. The PIMPLE algorithm is used to manage the velocity-pressure coupling. It is a combination of pressure implicit with splitting of operator (PISO) and semi-implicit method for pressure-linked equations (SIMPLE). The geometric algebraic multigrid (GAMG) preconditioner solver is used to solve the pressure while the preconditioned bi-conjugate gradient (PBiCG) solver is used to solve other variables.

Figure 2 shows the vertical profiles of the time-averaged streamwise velocity component (\bar{u}) normalized by the friction velocity (u_*), at four selected positions where u is the streamwise velocity component and overline represents time-averaged variables. In the comparisons, all LES results are found to agree reasonably well with the wind-tunnel measurements of Cheng and Castro (2002). Among the three LESs with different mesh resolutions, slight differences are found between the fine resolution case and the other two cases in the region above the cube array where larger values of \bar{u} are found in the fine resolution case. A possible reason is that grid independence is still not fully achieved for the results in that region. Another reason could be that the limited length and width of the current computational domain ($L_x = L_y = 1.2L_z$) are not large enough to resolve the large-scale motions in the turbulent boundary layer (Fang and Porté-Agel 2015), which may then induces errors in the

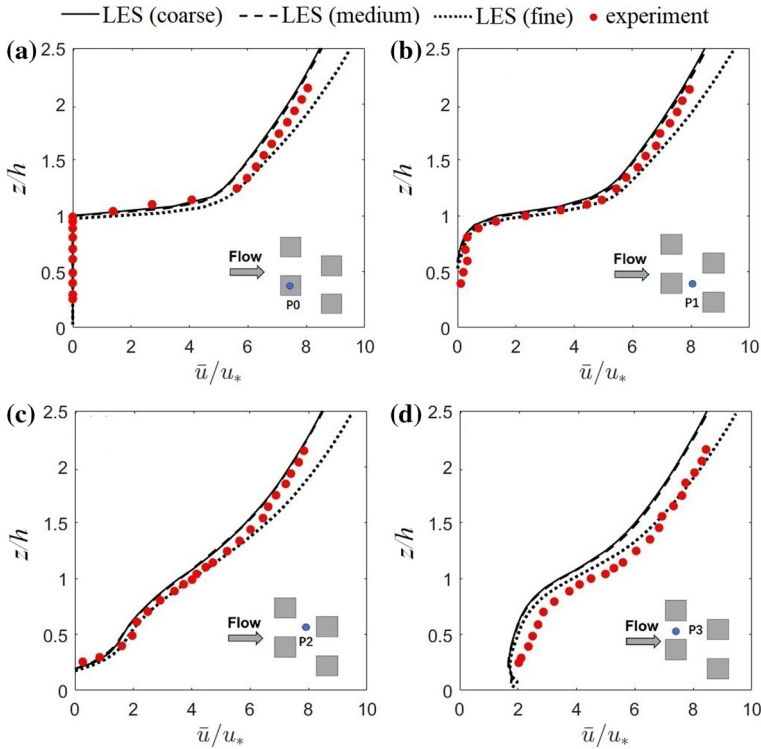


Fig. 2 Vertical profiles of the normalized mean streamwise velocity component (\bar{u}/u_*) at positions **a** P0, **b** P1, **c** P2, and **d** P3. Symbols: wind-tunnel measurements from Cheng and Castro (2002); lines: LES results

predicted wind profiles. Nevertheless, reasonable predictions of the mean winds within and above the urban canopy are found in all LESs.

In addition to \bar{u} , the turbulent vertical profiles of $\overline{u'u'}^{1/2}$, $\overline{w'w'}^{1/2}$ and $\overline{u'w'}^{1/2}$ at two selected positions are compared in Fig. 3, where u' and w' are the velocity fluctuations in the streamwise and vertical directions, respectively. In general, the results of all LESs agree reasonably well with the wind-tunnel measurements in all profiles. However, a peak in the profiles of $\overline{w'w'}^{1/2}$ at the position P1 (Fig. 3a) at the roof level of the cube array is found in the wind-tunnel measurements but not in the LESs. Similar results are also found in Xie and Castro (2016), who claimed that a finer mesh resolution is needed to resolve the peak. Moreover, for the profiles above the urban canopy, it is found that medium resolution case shows a slightly smaller value of $\overline{u'u'}^{1/2}$ than the other two cases, it is believed to be again due to the limited domain length in the x direction, which is not long enough to resolve the large-scale coherent structures in the turbulent boundary layer. Nevertheless, these results confirm that, by using roughly 12–16 grid points per building edge, reasonably good results of the mean wind and second-order turbulent statistics within the urban canopy can be obtained using the current LES method.

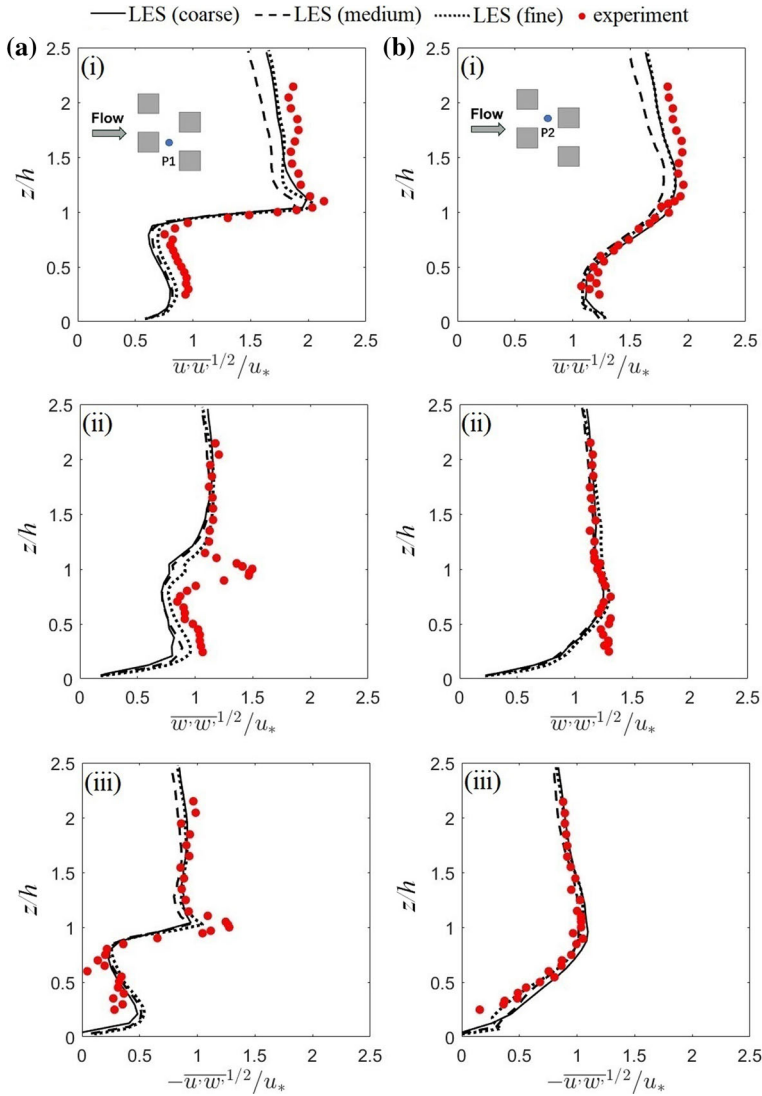


Fig. 3 Vertical profiles of the normalized (i) streamwise velocity standard deviation ($\overline{u'u'}^{1/2}/u_*$), (ii) vertical velocity standard deviation ($\overline{w'w'}^{1/2}/u_*$), and (iii) ($-\overline{u'w'}^{1/2}/u_*$) at **a** P1 and **b** P2. Symbols: wind-tunnel measurements from Cheng and Castro (2002); lines: LES results

3 Large-Eddy Simulations of Flow Over Realistic Urban Geometries

3.1 Urban and Terrain Data

After testing the performance in Sect. 2, the LES method is applied to simulate the flows over four realistic urban geometries. Open-source building map data of China cities are used to prepare the realistic urban geometries. In particular, four urban sites with areas of approximately 1000 m×500 m, are selected from three cities in the Guangdong Province of

China (Guangzhou, Zhongshan, and Shenzhen). The original building map data contain the information of the shapes and total floors of the buildings. To perform the LESs, the map data are converted into three-dimensional urban building models assuming that each floor has a height of 3 m based on the typical floor-to-floor heights for residential and commercial buildings in China. The computational domains for the four urban geometries are given in Fig. 4 with the plan-area fraction (Λ_p) given in Fig. 5. Λ_p is defined as the fraction of space occupied by buildings at a given horizontal plane (Giometto et al. 2016).

About the urban morphologies of the four cases, the urban surfaces in Cases 1 and 2 are characterized by large and tall buildings in the region. The values of H_{aver} and H_{max} for Case 1 (Case 2) are equal to 44.2 m (29.4 m) and 123 m (111 m), respectively (Table 1). Comparing the urban geometries of Cases 1 and 2, the building height and distribution for Case 1 are more homogeneous while in Case 2, taller buildings are more concentrated in one half of the region ($-400 \text{ m} < x < 0$) and shorter building in the other half ($0 < x < 400 \text{ m}$). This implies the higher urban geometry heterogeneity in Case 2. On the other hand, for Cases 3 and 4, it is found that most of the buildings are relatively short and dense (with $H_{aver} = 18.5 \text{ m}$ and 15.6 m , respectively). The values of H_{max} for Cases 3 and 4 are 84 m and 72 m, respectively, which are contributed by the particularly tall and large buildings in the regions for both cases. Note that similar building configurations of particular tall buildings towered on an urban surface with short and dense buildings are common in real cities. For this kind of surface, previous studies (Xie and Castro 2009; Moon et al. 2014; Hertwig et al. 2019; Cheng et al. 2021) found that the tall buildings can significantly affect the local urban flows. These four realistic urban geometries therefore can provide a variety of types of realistic urban geometries for flow characteristics analyses.

In all cases, to consider fully developed boundary-layer flows over the urban surfaces, periodic boundary conditions are used in the horizontal directions with a driven force F_x prescribed in the x direction throughout the fluid similar to the validation case. The top

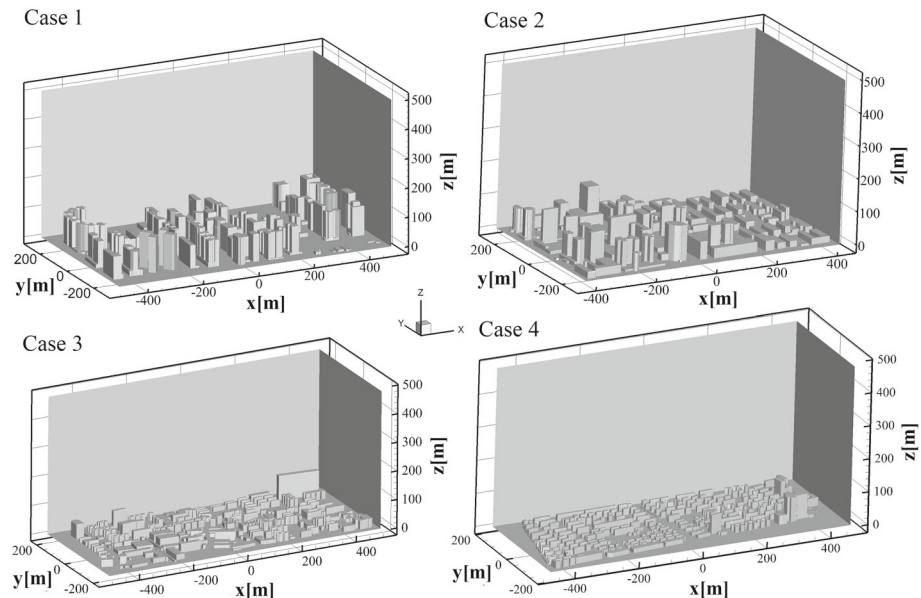


Fig. 4 Computational domains for the four LES cases of flows over realistic urban geometries

Fig. 5 Vertical profiles of the plan-area fraction (Λ_p) for the four realistic urban geometry cases. Dashed lines are the values of H_{aver} for the different cases and dotted line denotes $\Lambda_p = 0.02$

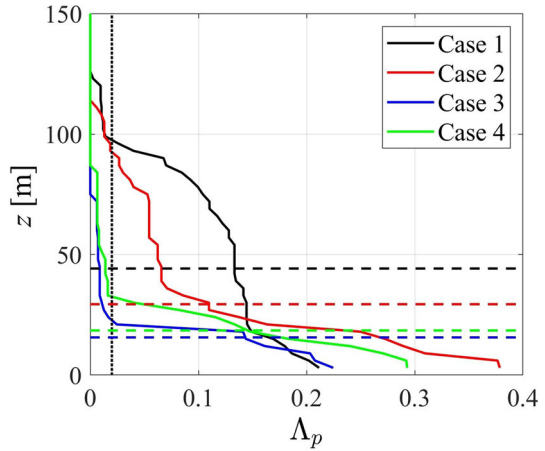


Table 1 Basic information of the four realistic urban geometry cases

Case	$L_x \times L_y \times L_z$	Total cells	H_{aver}	H_{max}
1	980 m \times 580 m \times 500 m	7351689	44.2 m	123 m
2	840 m \times 528 m \times 500 m	5451180	29.4 m	111m
3	1000 m \times 440 m \times 480 m	5174522	18.5 m	84 m
4	936 m \times 372 m \times 480 m	8764334	15.6 m	72 m

surface is considered as a stress-free wall while the building walls and the ground are no-slip walls with a wall function with $z_0 = 0.1$ m is used. The meshes, which are prepared using the OpenFOAM utility *snappyHexMesh*, are composed of mostly uniform hexahedral volume elements with each element having a volume of 4 m \times 4 m \times 4 m or less. Close to the building walls and ground, further mesh refinement with a minimum cell width of about 1 m is applied. The total numbers of cells for the four cases are provided in Table 1. Similar to the validation cases, flow statistics are collected after the LESs attain the quasi-steady state.

3.2 Overall Flow Patterns

3.2.1 Mean Flows

The overall flow patterns of the four realistic urban geometry cases are investigated in this section. Figure 6 shows the vertical contours of the normalized mean streamwise velocity component (\bar{u}/u_*) at selected planes of the four cases. In Cases 1 and 2, large wakes behind the buildings are found with lengths of more than 200 m. This, in turn, forms a relatively thick urban canopy layer with a height of about 100 m in both cases. In comparison, in Cases 3 and 4, only a relatively thin layer of recirculating flow (< 30 m) is found in most of the regions behind the short and dense buildings. Regarding the impacts of the particularly tall buildings in Cases 3 and 4, it is found that the wakes behind the tall buildings are relatively short with streamwise lengths less than 50 m compared with their building heights of 84 m and 72 m for Case 3 and 4, respectively. These wakes are much shorter than those found in Cases 1 and 2 behind the buildings of similar sizes. This is also different from what has been

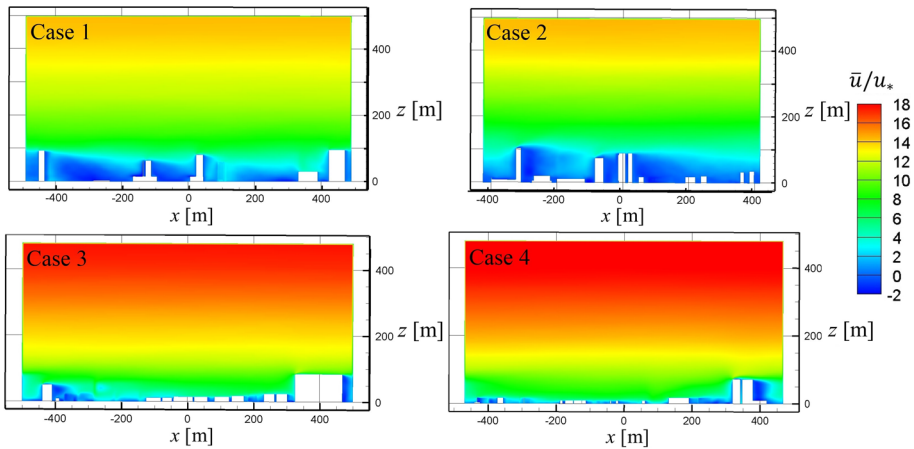


Fig. 6 Vertical contours of the normalized mean streamwise velocity component (\bar{u}/u_*) at selected planes in the realistic urban geometry cases. Case 1: $y = 200$ m; Case 2: $y = 20$ m; Case 3: $y = 164$ m; and Case 4: $y = -70$ m

found in Cheng et al. (2021) about the developing urban boundary layer over a realistic urban geometry of the Hong Kong urban area. The possible explanation is that fully developed urban boundary layers are considered in the current cases. The elevated turbulence intensity in the urban RSL thus increases the recovery of the wake behind tall buildings in Cases 3 and 4.

In addition to the wake pattern behind building, Fig. 6 also shows the higher value of U_0/u_* in Cases 3 and 4 ($U_0/u_* \sim 18$) than in Cases 1 and 2 ($U_0/u_* \sim 14$), where U_0 is the freestream wind speed. Note that u_*/U_0 is related to the square root of the drag coefficient (defined as $2u_*^2/U_0^2$, Garratt 1994) of the boundary layer. The higher values of U_0/u_* in Cases 3 and 4, therefore, imply the larger drag exerted by the urban geometries in Cases 1 and 2 than those in Cases 3 and 4. This is an expected result as the larger buildings in Cases 1 and 2 generally induce larger drags on the boundary-layer flows than the smaller buildings in Cases 3 and 4.

The horizontal contours of \bar{u}/u_* at $z = H_{\text{aver}}$ are also shown in Fig. 7. Consistent with the discussions of the vertical contours in Fig. 6, large wakes behind buildings are found in Cases 1 and 2. In particular, in Case 1, it is found that most of the region in the urban canopy layer is occupied by flow recirculations. By contrast, in Case 2, flow recirculations only occupy roughly about half of the area with relatively high wind speed regions still found in-between buildings. This is due to the increasing penetration of wind from above when the heterogeneity of urban geometry increases. On the other hand, in Cases 3 and 4, it is found that the overall wind speed is higher than those in Cases 1 and 2. Only small and short wakes are found behind the buildings due to the smaller size of the buildings in the areas. Moreover, significant increases in wind speed close to the particular tall buildings are found. A similar result is also found in the LES results of Moon et al. (2014) for the flow over a realistic urban geometry in Seoul, Korea.

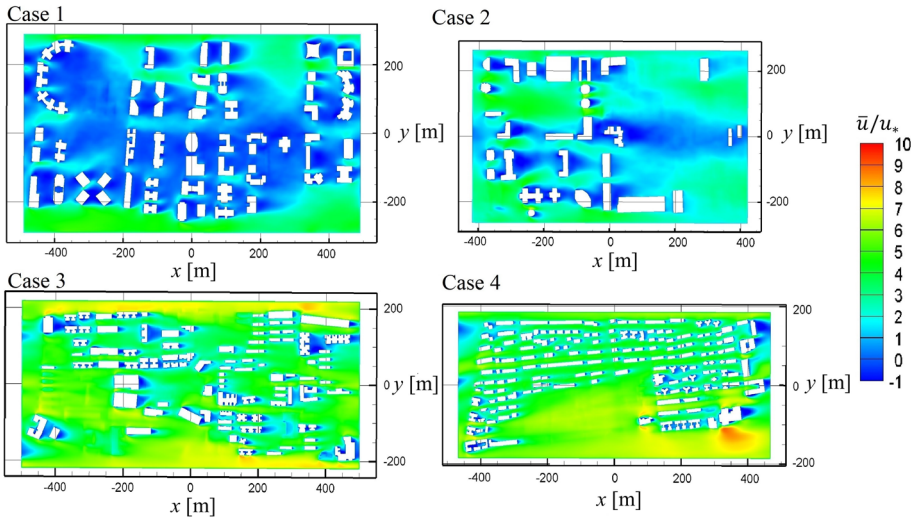


Fig. 7 Horizontal contours of the normalized mean streamwise velocity component (\bar{u}/u_*) at $z = H_{\text{aver}}$ in the realistic urban geometry cases

3.2.2 Turbulent Shear Stress

In addition to the mean streamwise velocity component, the vertical contours of the normalized turbulent shear stress $\overline{u'w'}/u_*^2$ (at the same vertical planes as in Fig. 6) are also compared in Fig. 8. In Case 1, a sharp development of shear layers growing at the roof level of buildings is found which causes a large negative value of $\overline{u'w'}/u_*^2 \approx -2$ in that region. Since the building height is relatively homogeneous in this case, the shear layer is found to maintain almost the whole domain length at $z \approx 100$ m. This pattern is similar to the results of staggered arrays of cubes of Cheng and Porté-Agel (2015). By contrast, in Case 2, the shear layers developed from the roof levels of the buildings are found to be not as sharp as those in Case 1. This is due to the larger variations of building height in this case. The maximum value of $\overline{u'w'}/u_*^2$ is also found to be smaller in Case 2 than in Case 1.

Different patterns of $\overline{u'w'}/u_*^2$ are found in Cases 3 and 4 in which strong shear layers, with lengths of about 100 to 200 m, are found to develop behind the particular tall buildings at the roof levels. Above the shorter and denser buildings in Cases 3 and 4, no apparent increment of the magnitudes of $\overline{u'w'}/u_*^2$ is found in both cases. This is consistent with the results of Blunn et al. (2022) that the flows in the lower region are sheltered from the shear layer formed at the roof level of the tall buildings.

3.3 Time- and Horizontally Space-Averaged Statistics

After understanding the overall mean flow and turbulence characteristics in the four realistic urban geometry cases, the LES results are further analyzed in this section to provide information for urban flow parametrizations. In particular, the time- and horizontally space-averaged statistics, with the horizontal space averages covering the whole computational domain (denoted by $\langle \cdot \rangle$), are calculated for the four cases. Extrinsic average (also known as the superficial or comprehensive average) is used, where quantities are normalized by the

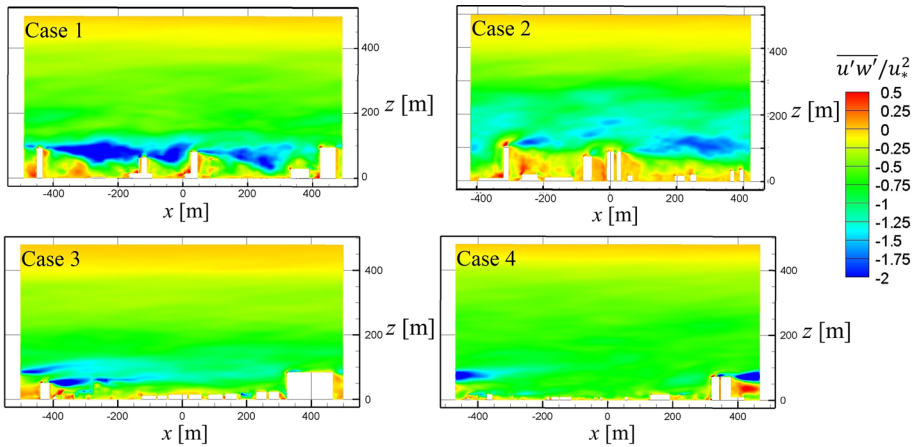


Fig. 8 Vertical contours of the normalized mean turbulent shear stress ($\overline{u'w'}/u_*^2$) at selected planes in the realistic urban geometry cases. Case 1: $y/m= 200$; Case 2: $y/m= 20$; Case 3: $y/m= 164$; and Case 4: $y/m= -70$

total volume including solid canopy elements. This averaging method has been applied in the previous studies of urban canopy flows (Castro 2017; Xie and Fuka 2018; Schmid et al. 2019).

3.3.1 Mean Wind Profiles

Figure 9a shows the vertical profiles of the time- and horizontally space-averaged streamwise velocity component for the four cases. It is found that all profiles can be characterized by an inflection point at a height (H_i) which can be interpreted as the height of the urban canopy (Oke et al. 2017). Consistent with the discussions in Sect. 3.2. The values of H_i are found to be larger in Cases 1 and 2 than those in Cases 3 and 4, which is related to the deeper urban canyon layers in the first two cases. For comparison, the positions of H_{aver} and H_{max} for all cases are also shown in Fig. 9a by the solid lines and dashed lines, respectively. It is found that, in all cases, H_i is located between H_{aver} and H_{max} . This is consistent with the results of Xie et al. (2008) and Giometto et al. (2016), which showed that H_i is located between H_{aver} and H_{max} . These results, therefore, imply that neither H_{aver} nor H_{max} is a good representation of the height of realistic urban canopies.

In addition to the mean wind profiles, the vertical profiles of the time- and horizontally space-averaged turbulent ($\overline{\langle u'w' \rangle}$) and dispersive ($\overline{\langle \tilde{u}\tilde{w} \rangle}$) momentum fluxes for the four cases are shown in Fig. 9b, where $\tilde{u} = \bar{u} - \langle \bar{u} \rangle$ and $\tilde{w} = \bar{w} - \langle \bar{w} \rangle$ are the spatial variations of the streamwise and vertical time-averaged velocity components, respectively. Different from the locations of the inflection point found in the $\langle \bar{u} \rangle$ profiles, the maximum magnitude of $\overline{\langle u'w' \rangle}$ is found approximately at H_{max} in all cases. This can be explained by the results in Fig. 8 that the largest turbulent momentum flux is found at the roof level of the tall buildings. This result is again consistent with Xie et al. (2008) in which turbulent momentum flux peaked at H_{max} is also found. However, Giometto et al. (2016) found that turbulent momentum flux peaks below H_{max} . This could be due to the tallest building in their cases only occupies a modest fraction of the region.

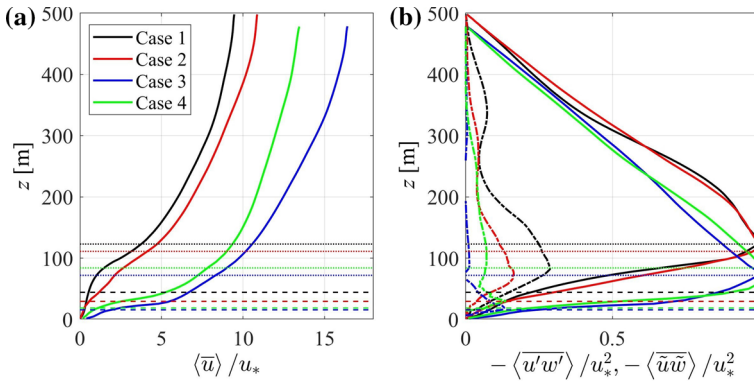


Fig. 9 Vertical profiles of the normalized time- and horizontally space-averaged **a** streamwise velocity component ($\langle \bar{u} \rangle / u_*$), and **b** turbulent ($-\langle u'w' \rangle / u_*^2$) (solid lines) and dispersive ($-\langle \tilde{u}\tilde{w} \rangle / u_*^2$) (dashed dot lines) momentum fluxes. Dashed and dotted lines represent the values of H_{aver} and H_{max} , respectively, for the different cases

On the other hand, the largest dispersive momentum flux is found in Case 1 followed by Case 2 with peak magnitudes equal to $0.25u_*^2$ and $0.2u_*^2$, respectively. This is believed to be related to the stronger recirculating flow within the urban canopies found in Cases 1 and 2 than those in Cases 3 and 4 (Fig. 6). In all cases, the magnitude of the dispersive flux is found to be peaked at a position between H_{aver} and H_{max} but is slightly lower than H_i . This result is different from Giometto et al. (2016) in which the dispersive momentum flux is found to be peaked at H_{aver} , but H_i is only slightly higher than H_{aver} in their cases. More discussions on the magnitudes of the dispersive momentum fluxes compared with the turbulent momentum fluxes would be given in Sect. 3.3.3.

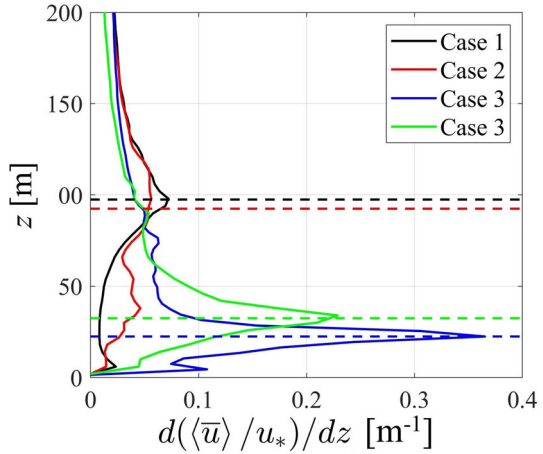
3.3.2 Normalization Height for Urban Canopies

The height of the urban canopy layer is an important parameter in UCMs. However, the position of the inflection point in the $\langle \bar{u} \rangle$ profile is generally not known before conducting building-resolved experimental or simulation studies. Therefore, for developing urban flow parametrizations, it would be meaningful to have a simple method that can predict the heights of urban canopy layers based on urban morphology parameters. Based on the current LES results, a simple criterion is proposed to predict urban canopy height as:

$$A_p|_{z=H_\lambda} = A_c, \tag{1}$$

where H_λ is the predicted urban canopy height and $A_c = 0.02$ is a threshold value chosen based on the current LESs. The rationale behind this criterion is that the impact of tall buildings is only significant when A_p is larger than A_c . To identify the value of H_λ of the current cases, the line of $A_p = 0.02$ is plotted in Fig. 5 and its intersection points with the four A_p curves therefore denote the predicted values of H_λ . To test the performance of this criterion, Fig. 10 shows the profiles of the vertical gradient of $\langle \bar{u} \rangle$ in the different cases. The locations of inflection points can be identified by the local maximum in the profiles while the predictions of Eq. 1 are shown by the dashed lines. It shows that using Eq. 1 gives good predictions of the locations of the inflection point heights for the current realistic urban geometry cases.

Fig. 10 Vertical profiles of the normalized vertical velocity gradient $(d(\langle \bar{u} \rangle / u_*) / dz)$ (solid lines) and the predicted values of H_λ for the different cases (dashed lines)



In order to further test the performance of using H_λ as the normalization length scale, the vertical profiles of $\langle \bar{u} \rangle / u_*$ against z normalized by H_λ , H_{aver} and H_{max} are shown in Fig. 11. In addition to the current results, the LES results of Xie et al. (2008) for a staggered array of random height building blocks and Giometto et al. (2016) for the flows above realistic urban geometry in Basel, Switzerland with two different wind directions are also included in Fig. 11. These data are directly extracted from their articles and values of H_λ are estimated from the urban geometries provided. In addition, the LES result of Cheng and Porté-Agel (2021) for the flow over a uniform staggered array of cubes of $\lambda_p = 0.25$ is also included as a reference case for an idealized urban canyon. Note that, for a uniform array of cubes, H_λ equals the height of the cubes (H). Also, for the results of Giometto et al. (2016), the intrinsic averaging method is used to calculate the vertical profiles, which would lead to the profiles to have a larger magnitudes (by a factor of $1/(1 - \Delta_p)$) than those calculated by the extrinsic averaging method.

The comparison shows that after using H_λ as the normalization height, profiles for all cases collapse approximately on the same curve (Fig. 11a) and the inflection point locations in all the cases are found to be located roughly at $z/H_\lambda = 1$. This supports the use of H_λ as the normalization scale. By contrast, when using H_{aver} as the normalization scale (Fig. 11b), it is found that large differences in the wind profiles among different cases exist, which implies that H_{aver} is a poor representation of urban canopy height. Besides, for H_{max} (Fig. 11c), it is found that only the case of Xie et al. (2008) and current Cases 1 and 2 agree well with that of the idealized uniform urban canyon case, while poor agreements are found for the two cases of Giometto et al. (2016) and the current Cases 3 and 4. Note that both the Giometto et al. (2016) cases and the current Cases 3 and 4 are characterized by the presence of particularly tall buildings on top of shorter buildings. This result may therefore suggest that, in this condition, H_{max} cannot be used as the representative height for realistic urban geometries.

3.3.3 Dispersive Stresses

After identifying the normalization heights for the urban canopies, the dispersive momentum flux, which is caused by the spatial heterogeneity of the mean wind, is discussed in this section. The vertical profiles of the horizontally space-averaged dispersive momentum flux $(-\langle \tilde{u} \tilde{w} \rangle)$ for the four realistic urban geometry cases are shown in Fig. 12a together with

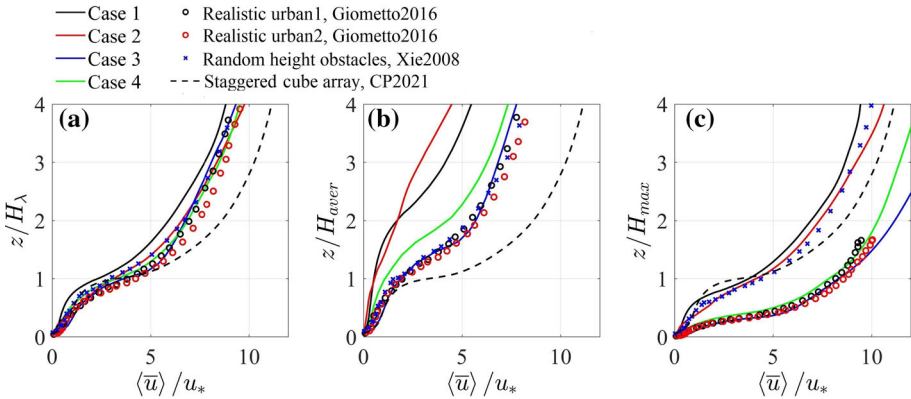


Fig. 11 Vertical profiles of time- and horizontally space-averaged streamwise velocity component $\langle \bar{u} \rangle / u_*$ against z normalized by **a** H_λ , **b** H_{aver} , and **c** H_{max} for the different cases. Lines: current LESs; Circles: LESs of Giometto et al. (2016); Crosses: LES of Xie et al. (2008); Dashed lines: LES of Cheng and Porté-Agel (2021) (CP2021)

the results of Xie et al. (2008) and Giometto et al. (2016) for comparison. It is found that $\langle \tilde{u}\tilde{w} \rangle$ is negative in most of the regions within urban canopies in all cases. In addition, the profiles are found to peak at the heights of $\approx 0.6 - 0.9H_\lambda$. Except for the region close to the ground surface, $-\langle \tilde{u}\tilde{w} \rangle$ is found to increase almost linearly below the peak in all cases. The magnitude of the flux is found to be sensitive to the building geometry with the largest peak value of $0.29u_*^2$ is found in Case 1 and in the results of Giometto et al. (2016). In comparison, smaller magnitudes of the peak values of about $0.13u_*^2$ are found in the other cases. The larger magnitude of $\langle \tilde{u}\tilde{w} \rangle$ found in Case 1 can be explained by the stronger recirculation flow found in that case. Besides, in the results of Giometto et al. (2016), $-\langle \tilde{u}\tilde{w} \rangle$ is found to decrease quickly with height in the region $0.6 < z/H_\lambda < 1$ and attain a local minimum value just above H_λ . By contrast, in the current cases, $-\langle \tilde{u}\tilde{w} \rangle$ is found to decrease much more slowly and roughly linearly above H_λ up to a height $> 2H_\lambda$. A similar pattern is also found in the result of Xie et al. (2008) but with a faster decreasing rate until $z = 1.5H_\lambda$. The cause for these different patterns among the different results is currently unclear. It is also noteworthy to point out that the intrinsic averaging method is used in Giometto et al. (2016) to calculate the dispersive flux which could also lead to different profile patterns than those calculated by the extrinsic method.

In addition to the dispersive momentum flux profiles, the ratio between dispersive momentum flux and turbulent momentum flux for the four realistic urban geometry cases are also compared in Fig. 12b together with the result of Leonardi and Castro (2010) for the staggered array of cubes (idealized urban geometry) with $\lambda_p = 0.25$. Similar patterns between the realistic and idealized uniform canopies are found with peaked values of the ratio located approximately at $z/H_\lambda = 0.4$. Within the urban canopies ($z/H_\lambda < 1$), it is found that the magnitudes of $\langle \tilde{u}\tilde{w} \rangle / \langle \overline{u'w'} \rangle$ for the idealized and realistic cases are comparable. Among all the cases, largest magnitude of $\langle \tilde{u}\tilde{w} \rangle / \langle \overline{u'w'} \rangle$ is found in Case 1 with value up to 0.68 at $z/H_\lambda = 0.43$, and smallest value is found in Case 4 with peak value of about 0.3 at $z/H_\lambda = 0.55$. This implies that the dispersive momentum flux is non-negligible within canopies in all cases. Besides, a change in the slope of $\langle \tilde{u}\tilde{w} \rangle / \langle \overline{u'w'} \rangle$ profile is found at $z/H_\lambda = 1$ in all cases. For the idealized staggered cube array, $\langle \tilde{u}\tilde{w} \rangle / \langle \overline{u'w'} \rangle$ is found to be

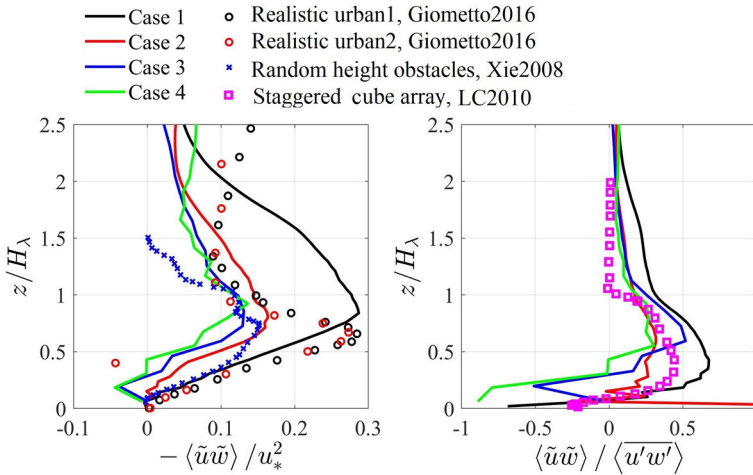


Fig. 12 Vertical profiles of **a** the dispersive momentum flux ($-\langle \tilde{u}\tilde{w} \rangle / u_*^2$) and **b** the ratio between dispersive and turbulent momentum fluxes ($\langle \tilde{u}\tilde{w} \rangle / \langle u'w' \rangle$). Lines: current LESs; Circles: LESs of Giometto et al. (2016); Crosses: LES of Xie et al. (2008); Squares: DNS of Leonardi and Castro (2010)

almost zero above H_λ , while for the realistic geometries, non-zero values of $\langle \tilde{u}\tilde{w} \rangle / \langle u'w' \rangle$ are found up to $2.5H_\lambda$. This result further supports the use of H_λ as the representative urban canopy height.

3.3.4 Effective Mixing Length

Using mixing length model to parametrize the time- and horizontally space-averaged turbulent momentum flux within and above urban canopies is a common method in UCMs (Macdonald 2000; Coceal and Belcher 2004; Cheng and Porté-Agel 2021). The effective mixing length (l_m) above urban surfaces is expected to be functions of z and urban geometries (Castro 2017; Cheng and Porté-Agel 2021; Blunn et al. 2022). Its behaviour for the four realistic urban geometry cases are discussed in this section. l_m can be defined by the equation:

$$\langle u'w' \rangle = - \left(l_m(z) \frac{\partial \langle \bar{u} \rangle}{\partial z} \right)^2 \tag{2}$$

As discussed in Sect. 3.3.3, dispersive stress is found to be non-negligible in urban canopies, and there is a recent attempt (Castro 2017) to include the dispersive stress in the calculation of the effective mixing length (l'_m) as:

$$\langle u'w' \rangle + \langle \tilde{u}\tilde{w} \rangle = - \left(l'_m(z) \frac{\partial \langle \bar{u} \rangle}{\partial z} \right)^2 \tag{3}$$

Figure 13a shows the vertical profiles of l_m (solid lines) and l'_m (dashed lines) for the different realistic urban geometry cases normalized by H_λ . In addition, the results of l_m for the staggered arrays of cubes of $\lambda_p = 0.111, 0.174$ and 0.25 from Cheng and Porté-Agel (2021) are also shown in Fig. 13b for comparison. It is found that for the realistic urban geometry cases, l_m and l'_m are very similar at all heights for all the realistic geometry cases

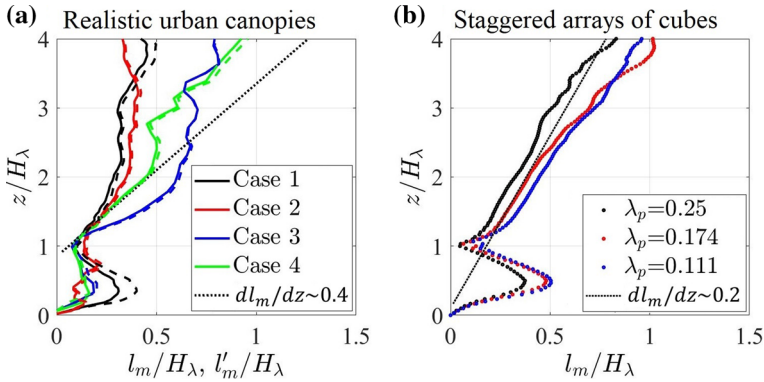


Fig. 13 Vertical profiles of the effective mixing length (l_m) for the different cases: **a** current LESs (solid lines: l_m ; dashed lines: l'_m) and **b** LESs of Cheng and Porté-Agel (2021)

except Case 1 in which larger values of l'_m than l_m (about 25% larger in the peak value) is found within the canopy. This is related to the larger dispersive stress found in Case 1. Comparing the shape of l_m profiles between realistic and idealized urban geometries, it is found that, within urban canopies ($z < H_\lambda$), l_m in realistic urban canopies show similar patterns to that of idealized urban canopies. In particular, a local minimum is found at $z = H_\lambda$ while a local maximum is found approximately at the middle height of the urban canopy for Cases 1, 3, and 4. These results also support that H_λ is a reasonable representation of the urban canopy heights. For Case 2, the l_m profile is more scattered below H_λ and l_m can be roughly assumed to be uniform with height.

Compared with the l_m results for staggered arrays of cubes, it is found that the slopes of l_m , for the realistic urban geometry cases, are smaller in magnitudes (less negative) in the region $0.5 < z/H_\lambda < 1$. This is because of the high variations in building heights in the realistic urban geometry cases (especially in Case 2), which make the shear layer at the roof level not as sharp as those in the idealized cases. Also note that l_m is currently normalized by H_λ in Fig. 13, which may not be the correct normalization for l_m especially at the high shear region close to $z = H_\lambda$. Since for very deep urban canopies, the ground surface would be expected to have negligible impact on the shear layer at the roof level. In this case, l_m would not be expected to scale with H_λ .

Recently, Blunn et al. (2022) found that, in the inertial sublayer above idealized urban geometries, the von Kármán constant (κ) shows a large variation in values from 0.20 to 0.51. It is therefore of interest to estimate the values of κ for the different cases from the l_m profiles. The value of κ can be estimated in Fig. 13 from the slope of l_m in the inertial sublayer (Coccal et al. 2006; Cheng and Porté-Agel 2021) as:

$$l_m = \kappa (z - d). \tag{4}$$

Figure 13b shows that for the uniform staggered arrays of cubes, a value of $\kappa \sim 0.2$ is found in all three cases. This is consistent with the results of Castro and Leonardi (2010) and Leonardi and Castro (2010), which showed the value of κ is lower than the classical value of 0.4 for staggered arrays of cubes. On the other hand, for the realistic urban geometry cases, it is found that the values of κ can be given by the classical value of 0.4 although the l_m profiles are much more scattered (Fig. 13c). However, it is necessary to point out that the current domain sizes in the horizontal directions are smaller than the suggested standard values of

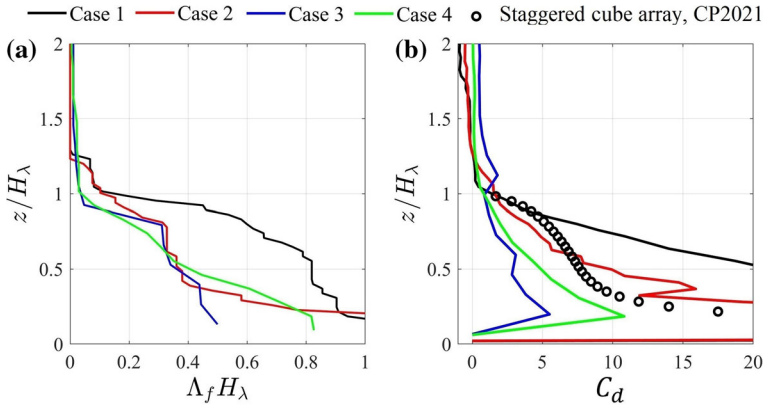


Fig. 14 Vertical profiles of the **a** sectional frontal area density (Λ_f) and **b** sectional drag coefficient (C_d) for the different cases. Lines: current LESs; Symbols: LES of Cheng and Porté-Agel (2021)

$L_x = L_y = 2\pi L_z$ for boundary-layer flows (see Fang and Porté-Agel (2015) for example), which may affect the results of l_m profiles in the above-canopy layer region. In addition, further assessment to make sure that the LES method is able to accurately reproduce the turbulence statistics in the boundary layer is necessary (Giacomini and Giometto 2021).

3.3.5 Sectional Drag Coefficient

In addition to l_m , the sectional drag coefficient (C_d) (Macdonald 2000), which is an important parameter in UCMs, is calculated for the different cases. For urban surfaces with variable building heights, a sectional frontal area density (Λ_f) can be defined as:

$$\int_0^{H_{\max}} \Lambda_f(z) dz = \lambda_f, \tag{5}$$

where $\Lambda_f(z)$ has a dimension of the reciprocal of length, representing the sum of the widths of all the building frontal surfaces at a height z divided by the total ground surface area. Using this definition, C_d can be obtained by the equation:

$$D(z) = \frac{1}{2} C_d(z) \Lambda_f(z) \langle \bar{u}(z) \rangle | \langle \bar{u}(z) \rangle |, \tag{6}$$

where D is the canopy drag force at height z . For uniform building block arrays, $H_{\max} = H$ and $\Lambda_f(z)$ is uniform with height equal to λ_f/H . Here, D is calculated from the balance of momentum in the x direction (Leonardi and Castro 2010) based on the time- and horizontally space-averaged momentum equation:

$$D(z) = -\frac{\partial \langle \overline{u'w'} \rangle}{\partial z} - \frac{\partial \langle \tilde{u}\tilde{w} \rangle}{\partial z} + F_x, \tag{7}$$

where the viscous term is ignored (Leonardi and Castro 2010).

Figure 14 shows the vertical profiles of Λ_f and C_d for the four realistic urban geometries. The result of C_d for the staggered array of cubes of $\lambda_p = 0.25$ from Cheng and Porté-Agel (2021) is also included in Fig. 14b for comparison. It is found that the C_d profiles of the four realistic urban geometry cases show similar patterns like those found in the idealized urban canopy case. In particular, C_d is found to decrease with height within canopies in all cases,

and small negligible values are found above H_λ . These results again support that H_λ is a reasonable estimation of the urban canopy height. Among the four realistic urban geometry cases, Case 1 is found to have the largest overall magnitude of C_d , followed by Cases 2, 3, then 4. This is consistent with the discussion in Sect. 3.2 that a lower wind speed is found within urban canopy for Case 1 (Fig. 9).

4 Conclusions

In this study, a large-eddy simulation (LES) method is used to study the flow characteristics over realistic urban geometries. The accuracy and grid sensitivity of the LES results are first tested with wind tunnel measurements for a staggered array of cubes of plane area density = 0.25. It is found that using roughly 12–16 grid points per building edge is enough for obtaining reasonable results of the mean wind and second-order statistics of the flow field. The LES method is then used to perform the simulations of flows over four different realistic urban geometries each with a surface area of $\sim 1000 \text{ m} \times 500 \text{ m}$. The building map data are obtained from three cities (Guangzhou, Zhongshan, and Shenzhen) in Guangdong, China. Two of the cases are characterized by taller and larger buildings in the areas while the other two by shorter and denser buildings with the presence of particularly tall buildings in the areas.

The overall patterns of the mean streamwise velocity component (\bar{u}) and the turbulent momentum flux ($\overline{u'w'}$) for the four cases are first investigated. Due to the taller and bigger buildings in Cases 1 and 2, thicker urban canyon layers are found in these cases which have also exerted larger drags on the flows compared with those in Cases 3 and 4. In addition, in Cases 3 and 4, the flow close to the dense and short buildings is found to be sheltered by the shear layer formed at the roof level of the particularly tall buildings.

To provide information for developing urban flow parametrizations, the time- and horizontally space-averaged profiles of the streamwise velocity component ($\langle \bar{u} \rangle$), turbulent momentum flux ($\langle \overline{u'w'} \rangle$), dispersive momentum flux ($\langle \tilde{u}\tilde{w} \rangle$), effective mixing length (l_m), and sectional drag coefficient (C_d) are examined. In particular, based on the plan area fraction of the urban geometries, a new simple criterion is proposed to predict the urban canopy height (denoted by H_λ). By comparing the $\langle \bar{u} \rangle$ profiles from the current LES results with the other existing data in the literature for both realistic and idealized urban geometries, it is found that H_λ is a better representation of the urban canopy height than the average building height and the maximum building height. Moreover, by using H_λ to normalize the vertical coordinate, consistent patterns are found among the realistic and idealized urban geometries in the profiles of $\langle \tilde{u}\tilde{w} \rangle$, l_m and C_d . These results would be meaningful for the development of parametrizations of flows over realistic urban geometries.

Besides, the magnitudes of dispersive momentum flux are found to be equal to about 30–66% of that of the turbulent momentum flux within urban canopies for the different cases. However, the effect of dispersive momentum flux on l_m is found to be only important in the case with the largest dispersive momentum flux. In this case, l_m is found to increase by about 25% within canopies. The values of von Kármán constant (κ) are also estimated from the l_m profiles for the current cases and the cases of staggered arrays of cubes from Cheng and Porté-Agel (2021). Consistent with earlier studies, values of $\kappa \approx 0.2$ smaller than the classical value of 0.4 are found for the staggered arrays of cubes. In comparison, in the realistic urban geometry cases, values of κ close to the classical value are found although the l_m profiles are more scattered in these cases. However, more experimental and simulation

data in the roughness and inertial sublayers over urban surfaces are needed to confirm this finding.

The current analyses of flows over realistic urban geometries would be useful to understand the impacts of urban geometry heterogeneity on the mean wind and turbulence characteristics. Future works will further quantify the effects of realistic urban geometries on the profiles of dispersive stress, effective mixing length, and section drag coefficient, in order to improve the current flow parametrizations in urban canopy models.

Acknowledgements This study is supported by the National Natural Science Foundation of China and Macau Science and Technology Development Joint Fund (NSFC-FDCT), China and Macau (41861164027) and the Fundamental Research Funds for the Central Universities, Sun Yat-sen University (2021qntd29). The authors would like to thank the anonymous reviewers for helpful comments.

Data availability The datasets generated during and/or analyzed during the current study are available from the corresponding author on reasonable request.

Declarations

Conflict of interest The authors have no competing interests to declare that are relevant to the content of this article.

References

- Barlow J, Coceal O (2009) A review of urban roughness sublayer turbulence. Technical Report, Met Office, Department of Meteorology, Reading University. p. 507
- Blunn LP, Coceal O, Nazarian N, Barlow JF, Plant RS, Bohnstengel SI, Lean HW (2022) Turbulence characteristics across a range of idealized urban canopy geometries. *Boundary-Layer Meteorol* 182:275–307
- Castro IP (2017) Are urban-canopy velocity profiles exponential? *Boundary-Layer Meteorol* 164:337–351
- Castro IP, Leonardi S (2010) Very-rough-wall channel flows: a DNS study. In: Nickels T (eds) IUTAM symposium on the physics of wall-bounded turbulent flows on rough walls IUTAM bookseries, vol 22
- Cheng H, Castro I (2002) Near wall flow over urban-like roughness. *Boundary-Layer Meteorol* 104:229–259
- Cheng WC, Liu CH (2011) Large-eddy simulation of flow and pollutant transports in and above two-dimensional idealized street canyons. *Boundary-Layer Meteorol* 139:411–437
- Cheng WC, Porté-Agel F (2015) Adjustment of turbulent boundary-layer flow to idealized urban surfaces: a large-eddy simulation study. *Boundary-Layer Meteorol* 155:249–270
- Cheng WC, Porté-Agel F (2021) A simple mixing-length model for urban canopy flows. *Boundary-Layer Meteorol* 181:1–9
- Cheng WC, Liu CH, Ho YK, Mo Z, Wu Z, Li W, Chan LYL, Kwan WK, Yau HT (2021) Turbulent flows over real heterogeneous urban surfaces: wind tunnel experiments and Reynolds-averaged Navier-Stokes simulations. *Build Simul* 14:1345–1358
- Coceal O, Belcher SE (2004) A canopy model of mean winds through urban areas. *Q J R Meteorol Soc* 130:1349–1372
- Coceal O, Thomas TG, Castro IP, Belcher SE (2006) Mean flow and turbulence statistics over groups of urban-like cubical obstacles. *Boundary-Layer Meteorol* 121:491–519
- Di Sabatino S, Solazzo E, Paradisi P, Britter R (2008) A simple model for spatially-averaged wind profiles within and above an urban canopy. *Boundary-Layer Meteorol* 127:131–151
- Fang J, Porté-Agel F (2015) Large-eddy simulation of very-large-scale motions in the neutrally stratified atmospheric boundary layer. *Boundary-Layer Meteorol* 155:397–416
- Garratt JR (1994) *The atmospheric boundary layer*, 3rd edn. Cambridge University Press, Cambridge, p 336
- Giacomini B, Giometto MG (2021) On the suitability of second-order accurate finite-volume solvers for the simulation of atmospheric boundary layer flow. *Geosci Model Dev* 14:1409–1426
- Giometto MG, Christen A, Meneveau C, Fang J, Krafczyk M, Parlange MB (2016) Spatial characteristics of roughness sublayer mean flow and turbulence over a realistic urban surface. *Boundary-Layer Meteorol* 160:425–452

- Grimmond CSB, Oke TR (1999) Aerodynamic properties of urban areas derived from analysis of surface form. *J App Meteorol* 38:1262–1291
- Hertwig D, Gough HL, Grimmond S, Barlow JF, Kent CW, Lin WE, Robins AG, Hayden P (2019) Wake characteristics of tall buildings in a realistic urban canopy. *Boundary-Layer Meteorol* 172:239–270
- Kanda M, Inagaki A, Miyamoto T, Gryschka M, Raasch S (2013) A new aerodynamic parametrization for real urban surfaces. *Boundary-Layer Meteorol* 148:357–377
- Kono T, Tamura T, Ashie Y (2010) Numerical investigations of mean winds within canopies of regularly arrayed cubical buildings under neutral stability conditions. *Boundary-Layer Meteorol* 134:131–155
- Leonardi S, Castro IP (2010) Channel flow over large cube roughness: a direct numerical simulation study. *J Fluid Mech* 651:519–539
- Li XX, Liu CH, Leung DYC, Lam KM (2006) Recent progress in CFD modelling of wind field and pollutant transport in street canyons. *Atmos Environ* 40:5640–5658
- Macdonald RW (2000) Modelling the mean velocity profile in the urban canopy layer. *Boundary-Layer Meteorol* 97:25–45
- Macdonald RW, Griffiths RF, Hall DJ (1998) An improved method for the estimation of surface roughness of obstacle arrays. *Atmos Environ* 32:1857–1864
- Moon K, Hwang JM, Kim BG, Lee C, Choi J (2014) Large-eddy simulation of turbulent flow and dispersion over a complex urban street canyon. *Environ Fluid Mech* 14:1381–1403
- Nazarian N, Kravayehoff ES, Martilli A (2020) A one-dimensional model of turbulent flow through “urban” canopies (mlucm v2.0): updates based on large-eddy simulation. *Geosci Model Dev* 13:937–953
- Oke TR, Mills G, Christen A, Voogt JA (2017) *Urban climates*. Cambridge University Press, Cambridge, p 519
- OpenFOAM (2018) User guide. OpenFOAM
- Raupach MR, Finnigan JJ, Brunei Y (1996) Coherent eddies and turbulence in vegetation canopies: the mixing-layer analogy. *Boundary-Layer Meteorol* 78:351–382
- Santiago JL, Martilli A (2010) A dynamic urban canopy parameterization for mesoscale models based on computational fluid dynamics Reynolds-averaged Navier-Stokes microscale simulation. *Boundary-Layer Meteorol* 137:417–439
- Schmid MF, Lawrence GA, Parlange MB, Giometto MG (2019) Volume averaging for urban canopies. *Boundary-Layer Meteorol* 173:349–372
- Schumann U (1975) Subgrid scale model for finite difference simulations of turbulent flows in plane channels and annuli. *J Comput Phys* 18:376–404
- Spalding DB (1962) A new analytical expression for the drag of a flat plate valid for both the turbulent and laminar regimes. *Int J Heat Mass Transf* 5:1133–1138
- Sützl B, Rooney GG, van Reeuwijk M (2021) Drag distribution in idealized heterogeneous urban environments. *Boundary-Layer Meteorol* 178:225–248
- Xie ZT, Castro IP (2009) Large-eddy simulation for flow and dispersion in urban streets. *Atmos Environ* 43:2174–2185
- Xie Z, Castro IP (2016) LES and RANS for turbulent flow over arrays of wall-mounted obstacles. *Flow Turbulence Combust* 76:291–312
- Xie ZT, Fuka V (2018) A note on spatial averaging and shear stresses within urban canopies. *Boundary-Layer Meteorol* 167:171–179
- Xie ZT, Coceal O, Castro IP (2008) Large-eddy simulation of flows over random urban-like obstacles. *Boundary-Layer Meteorol* 129:1–23
- Yao L, Liu CH, Mo Z, Cheng WC, Bresseur GP, Chao CYH (2022) Statistical analysis of the organized turbulence structure in the inertial and roughness sublayers over real urban area by building-resolved large-eddy simulation. *Build Environ* 207B(108):464
- Yoshida T, Takemi T (2018) Properties of mixing length and dispersive stress in airflows over urban-like roughness obstacles with variable height. *SOLA* 14:174–178
- Zhu X, Iungo GV, Leonardi S, Anderson W (2017) Parametric study of urban-like topographic statistical moments relevant to a priori modelling of bulk aerodynamic parameters. *Boundary-Layer Meteorol* 162:231–253

Publisher's Note Springer Nature remains neutral with regard to jurisdictional claims in published maps and institutional affiliations.

Springer Nature or its licensor holds exclusive rights to this article under a publishing agreement with the author(s) or other rightsholder(s); author self-archiving of the accepted manuscript version of this article is solely governed by the terms of such publishing agreement and applicable law.